

Ion beam irradiation of ABO_4 compounds with the fergusonite, monazite, scheelite, and zircon structures

Massey de los Reyes¹ | Robert D. Aughterson¹  | Daniel J. Gregg¹  |
Simon C. Middleburgh^{1,4} | Nestor J. Zaluzec² | Ping Huai³ | Cuilan Ren³ |
Gregory R. Lumpkin¹ 

¹Australian Nuclear Science and Technology Organisation, Lucas Heights, NSW, Australia

²Photon Sciences Division, Argonne National Laboratory, Lemont, IL, USA

³Shanghai Institute of Applied Physics, Chinese Academy of Sciences, Shanghai, China

⁴Nuclear Futures Institute, Bangor University, Bangor Gwynedd, UK

Correspondence

Gregory R. Lumpkin, Australian Nuclear Science and Technology Organisation, Locked Bag 2001, Kirrawee DC, NSW 2232, Australia.
Email: grl@ansto.gov.au

Abstract

The effects of irradiation on $CaWO_4$, $SrWO_4$, $BaWO_4$, YVO_4 , $LaVO_4$, $YNbO_4$, and $LaNbO_4$ were investigated on thin crystals using 1.0 MeV Kr ions at 50–1000 K. All of the ABO_4 compounds can be amorphized with calculated damage cross sections ($\sigma_a = 1/F_{c0}$) in the range of $\sim 0.30\text{--}1.09 \times 10^{-14} \text{ cm}^2 \text{ ion}^{-1}$ at zero Kelvin. The analysis of fluence-temperature data returned critical temperatures for amorphization (T_c) of 311 ± 1 , 358 ± 90 , 325 ± 19 , 415 ± 17 , 541 ± 6 , 636 ± 26 , and 1012 ± 1 K, respectively, for the compounds listed above. Compared with previous in situ irradiation of ABO_4 orthophosphate samples using 0.8 MeV Kr ions, the T_c values of $LaVO_4$ and YVO_4 are higher than those of $LaPO_4$ and YPO_4 by 82 K and 124 K, respectively. The T_c values of the three scheelite structures, $CaWO_4$, $SrWO_4$, and $BaWO_4$, indicate that they are the most radiation tolerant compounds under these conditions. The A-B cation anti-site energies, E_{fAB} , determined by DFT range from 2.48 to 10.58 eV and are highly correlated with the A-B cation ionic radius ratio, r_A/r_B , but are not correlated with T_c across the different structure types, suggesting that the formation and migration energies of Frenkel defects play a more important role in damage recovery in these compounds. We also discuss the role of cation and anion charge/iconicity as determined by DFT. ABO_4 compounds with the zircon structure and $B = P$ or V have a distinct advantage over those with $B = Si$ as the damaged regions do not appear to be significantly affected by polymerization of $(PO_4)^{3-}$ or $(VO_4)^{3-}$ groups which might stabilize the amorphous fraction and ultimately lead to phase separation as observed in zircon ($ZrSiO_4$).

KEYWORDS

amorphization, fergusonite, ion irradiation, monazite, scheelite, zircon

1 | INTRODUCTION

The development of radiation-resistant materials has been an area of increasing interest over the years, particularly with the development of fusion and Generation IV nuclear reactors as potential contributors to sustainable future

energy.¹ In all reactor systems, the existence of both elevated temperatures and harsh irradiation environments are known to have a profound effect on core structural materials, causing the degradation and alteration of their physical and chemical properties.^{2,3} Similar problems also extend to candidate ceramic and glass-ceramic materials for nuclear

waste immobilization, experiencing radiation damage effects caused by the alpha decay of encapsulated plutonium and minor actinides.⁴⁻⁶

A great deal of effort has centered upon the mechanisms that govern radiation tolerance in materials, especially complex oxides. With the aid of ion beam irradiation techniques and validation from computer models, experimental investigations have focused primarily on understanding the cumulative decay processes of encapsulated radionuclides over time.⁷⁻⁹ In most cases, the degree of damage differs significantly as a function of composition and dose, with structural defects occurring due to varied phenomena that rely heavily upon the intricate balance between damage production, structural stability, ability to accommodate lattice disorder, and the energetics of defect formation and migration. In this regard, tailoring the response of materials to irradiation constitutes a major challenge in materials research; therefore, a fundamental understanding of a material's behavior under such conditions is necessary to justify its practical applicability.

Among a number of promising materials for nuclear waste immobilization, the ABO_4 compounds have gained significant interest, especially in the area of radiation tolerant crystalline host phases for actinides and fission products from spent nuclear fuel. The materials based on this general formula exhibit extensive chemical flexibility, with $A = Ca, Sr, Ba, Y,$ lanthanides, $Th,$ and U and $B = Si, P, As, Nb, Ta,$ and $W,$ among other elements. The most common ABO_4 compounds are based on the structures of fergusonite, monazite, scheelite, and zircon. These are also represented in nature as potential ores or minor carriers of $Nb, Ta, W, Y,$ lanthanides, $Th,$ and U in geological systems, enabling researchers to study the system evolution as a function of temperature, pressure, melt-fluid composition, and time.^{10,11} Radiation damage effects in these materials have been studied extensively, especially on zircon and monazite structured orthophosphates and silicates using ion irradiation techniques that cater specifically to the determination of damage models and mechanisms under strictly controlled conditions including temperature, ion mass, energy and flux.¹²⁻¹⁴ However, very little is known in regards to the radiation response of other ABO_4 structure types, particularly those with $B = V, Nb, W,$ and other elements apart from Si . In order to assess these materials for nuclear waste immobilization, this study aims at comparing the effects of ion beam irradiation on $CaWO_4, SrWO_4, BaWO_4, LaVO_4, YVO_4, LaNbO_4$ and $YNbO_4,$ spanning the various chemistries of ABO_4 compounds with either a monoclinic or tetragonal structure. This method aids in the identification of characteristic trends between different ABO_4 compounds due to the variation of structure/composition with respect to the critical amorphization dose (D_c) and

the critical temperature (T_c), above which the material remains crystalline.

2 | CRYSTAL CHEMISTRY OF ABO_4 STRUCTURE TYPES

This section is based in part on the review articles by Chakoumakous et al¹⁵ and Dacheux et al,¹⁶ together with a number of specific crystal structure refinements and other studies relevant to this work.¹⁷⁻²⁴ As shown in Figure 1, all four of the structure types in the system described above are composed of edge sharing 8 or 9 coordinated cation polyhedra (A-sites) and smaller isolated cation tetrahedra (B-sites) connected to the A-sites via either corner sharing (scheelite and fergusonite) or edge sharing (monazite and zircon). The zircon structure ($I4_1/amd$) is related to the monazite structure ($P2_1/n$) by a shift in the cation positions, rotation of anion positions about the tetrahedra, and the change in coordination of the A-site from 8 to 9. In zircon, there are two sets of four equal A-O bond lengths and four equal B-O bond lengths. However, the BO_4 tetrahedral sites are significantly distorted with two shorter shared O-O edges and four longer unshared O-O edges. Similarly, there are two O-B-O tetrahedral angles associated with the shared edges that are significantly smaller or greater than the ideal value of 109.5° and four associated with the unshared edges that are larger. In the monazite structure there are nine individual A-O bond lengths and four individual B-O distances. Like zircon, the two shared O-O edges are shorter and have the smaller O-B-O angles; however, due to the particular distortion of the BO_4 tetrahedron in monazite there are now only three angles significantly greater than 109.5° and one of which is close to this angle.

The crystal structure of scheelite (space group $I4_1/a$) consists of a framework of edge sharing AO_8 polyhedra connected to isolated BO_4 tetrahedra via corner sharing. There are two groups of four A-O distances in scheelite. All four B-O distances are equal; however, tetrahedron is somewhat distorted as shown by two sets of three O-B-O angles that are significantly smaller or larger than the ideal tetrahedral bond angle. Scheelite is related to fergusonite (standard space group $C2/c$, the non-standard space groups $I2/a$ or $I2/c$ are often used for comparison with scheelite) via small cation displacements and more significant changes in the anion positions. Phase transformations in fergusonite occur as a function of temperature and pressure and are generally of a second order, ferro-elastic type (Figure 2). In $YNbO_4$ and $LaNbO_4,$ the temperature driven phase transformations to scheelite occur at approximately 1073 and 790 K, respectively. Fergusonite, the low temperature or high-pressure phase, is effectively a “distorted and compressed” version of scheelite with four distinct pairs of A-O bond distances in

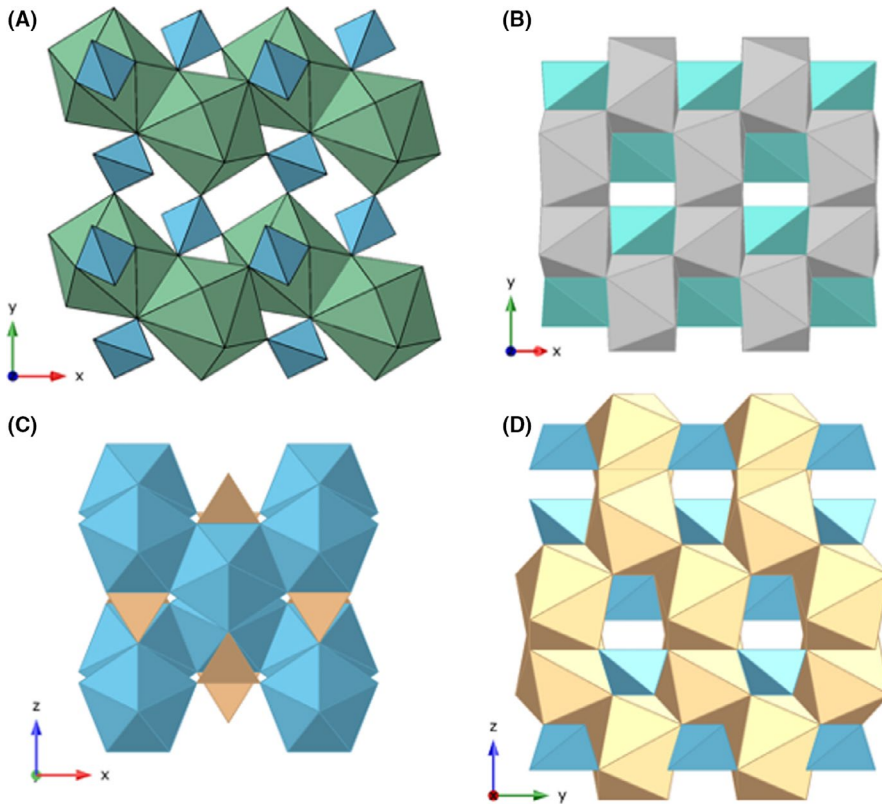


FIGURE 1 Crystal structure projections of (A) monazite on (001), (B) fergusonite on (001), (C) zircon on (010), and (D) scheelite on (100). Projections are chosen to place emphasis on differences in the cation polyhedral environments. In particular, note the large 9-fold coordinated A-site of monazite, the different morphology and symmetry aspects of the A-site in the other three structures, and the compressed tetrahedra and overall similarity of the A-B cation polyhedral framework of fergusonite (y-axis) and scheelite (z-axis) [Color figure can be viewed at wileyonlinelibrary.com]

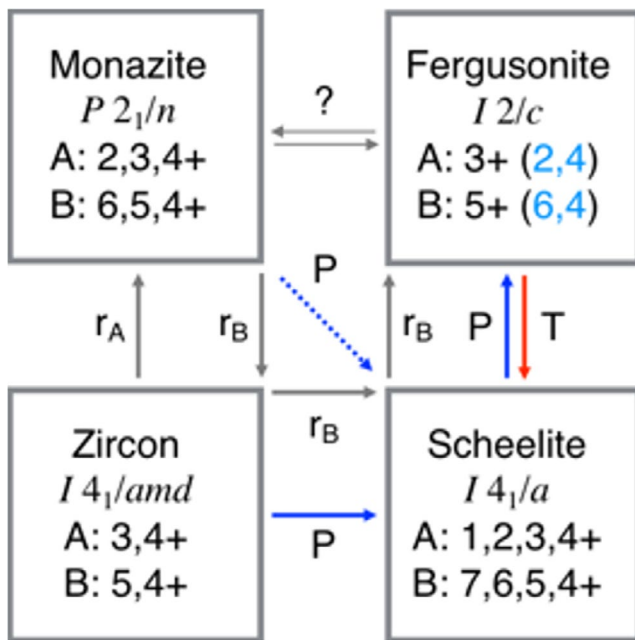


FIGURE 2 Schematic drawing showing the relationships between scheelite, monazite, zircon, and fergusonite in terms of temperature, pressure, and ionic radii based on the nominal compositions of the four structure types. The typical valence states of ions on the A- and B-sites are also shown. Laboratory synthesis of fergusonite typically involves A^{3+} and B^{5+} cations; light blue numbers in parentheses illustrate the other cation valence states found in natural fergusonite samples. P = pressure, T = temperature, r_A and r_B are the ionic radii of the A-site and B-site cations. Modified from AT Aldred⁵⁶ [Color figure can be viewed at wileyonlinelibrary.com]

the AO_8 polyhedron. Two of the oxygen atoms are displaced toward the B-site in fergusonite, therefore, the local coordination environment consists of two pairs of B-O distances (~ 1.8 and 1.9 Å) in a distorted tetrahedral configuration with another pair of distances at about 2.5 Å.

For these structure types, the cation-anion coordination environments can be expressed as $^{VIII}A^{IV}B^{III}O_4$ for zircon and scheelite, $^{IX}A^{IV}B^{III}O_3^{II}O$ for monazite, and either $^{VIII}A^{IV}B^{III}O_4$ or $^{VIII}A^{VI}B^{III}O_2^{II}O_2$ for fergusonite depending upon whether or not the B-site is considered to be IV or VI coordinated. Although in the latter case the choice is somewhat subjective, the configurations illustrated above point to important differences in the local coordination environments between these compounds. These local atomic configurations, coupled with differences in the chemistry of the B-site cation in particular, may have a major role in the atomic scale processes that affect the production and recovery of defects during irradiation, eg, the energetics of defect formation and migration on picosecond time scales.

3 | EXPERIMENTAL METHODS

3.1 | Materials synthesis

Polycrystalline ceramic samples of $CaWO_4$, $YNbO_4$, $LaVO_4$, and YVO_4 were prepared via conventional solid-state oxide methods using stoichiometric amounts of La_2O_3 (99.99%), Nb_2O_5 (99.99%), Y_2O_3 (99.99%), WO_3 (99%), V_2O_5 (99%),

and CaCO_3 (99%). Starting oxides were first calcined at 600°C for 10 hours and CaCO_3 was dried in an oven at 120°C before the powders were weighed then milled using Y_2O_3 -stabilized zirconia balls in Teflon containers in a cyclohexane media for 16 hours. The cyclohexane was evaporated from stainless steel pans at 110°C . The homogeneously mixed powder was then uniaxially pressed into pellets at 5 MPa, cold isostatically pressed (400 MPa for the tungstates and vanadates and 300 MPa for the niobates) and sintered for 16 hours at 1400°C for the niobates and tungstates and at 1100°C for the vanadates.

3.2 | Materials characterization

X-ray diffraction patterns were measured using a Bruker D8 instrument, with weighted $\text{CuK}\alpha$ radiation and a Sol-X detector. Samples were analyzed in the angular range of 10 - 80 degrees two theta, with a step size of 0.03° and a counting time of 10 seconds per step. A Zeiss Ultra Plus scanning electron microscope operating at 15 kV and equipped with an Oxford Instruments X-Max 80mm^2 SDD X-ray microanalysis system was used for microstructural and phase-composition analysis. Samples were mounted in an epoxy resin and polished to $1\ \mu\text{m}$ diamond finish. A carbon film ($\sim 5\ \text{nm}$) was deposited onto the polished surface for charge neutralization.

3.3 | Ion irradiation

Before irradiation, selected area diffraction patterns (SAED) were obtained using a JEOL 2010F transmission electron microscope (TEM) operated at an accelerating potential of 200 kV and calibrated for selected area diffraction over a range of objective lens currents using a gold film standard. TEM specimens were prepared by lightly grinding a small amount of powder dispersed in ethanol and drop casted by a plastic pipette onto holey carbon coated copper TEM grids and dried in air. Ion irradiation experiments with 1.0 MeV Kr ions were carried out in situ at the IVEM-Tandem User Facility at Argonne National Laboratory using a Hitachi TEM interfaced to a NEC ion accelerator.²⁵ All TEM observations were carried out using an accelerating potential of 300 kV. Ion irradiations were performed at temperature range of 50-1000 K with the electron beam of the TEM turned off, using a counting rate of 50 ion counts s^{-1} and a flux of 6.25×10^{11} ions $\text{cm}^{-2} \text{s}^{-1}$ within a beam of $\sim 2\ \text{mm}$ diameter. Each sample was irradiated using incremental irradiation steps and selected grains were observed using bright field imaging and selected area diffraction after each irradiation step. The critical amorphization fluence (F_c) was determined from the last fluence increment in which weak Bragg diffraction spots were observed and the next increment for which only diffuse

rings occur in the diffraction pattern. For each sample, F_c was determined from an average of 3 to 6 grains.

A zirconolite reference sample with previously established F_c was also irradiated in order to validate the experiments. The nominal thickness of the sample was determined by convergent beam electron diffraction to be approximately 60 nm. For this thickness most of the Kr ions pass through the sample.²⁶ Previously, we also discussed the effect of sample thickness on the number of displacements per ion generated as a function of thickness in similar pyrochlore samples.²⁷ If the actual thickness values are in the range of 40-80 nm then the displacements per ion will vary by a factor of approximately 2.0-2.5. This effect has been minimized by adopting a broad strategy wherein sample thickness is maintained at values close to that of the standard using a combination of image contrast and thickness contours in the TEM, complemented by observation of the X-ray count rates using energy-dispersive X-ray analysis.

3.4 | Monte carlo simulations of damage production

The irradiation damage to a TEM specimen by 1 MeV Kr ions was calculated using SRIM-2008 (Stopping and Range of Ions in Matter) with full damage cascades using the calculated densities obtained from the lattice parameters listed in Table 1.^{28,29} Here, displacement energies (E_d) of 50 eV were assumed for all atoms, coupled with surface binding energies of 3 eV in order to assess the effects of sample thickness and composition on defect production, stopping power, and energy transfer to atoms in the target. Traditionally, SRIM used lower default values of E_d while giving the user the option to use a value of their choice. However, in the late 1990's the E_d values for a few simple oxides were reasonably well known, eg, Al_2O_3 ($E_d^{\text{O}} \sim 50$ -60 and $E_d^{\text{Al}} \sim 20$ -30 eV), MgO ($E_d^{\text{O}} \sim 50$ and $E_d^{\text{Mg}} \sim 60$ eV), ZnO ($E_d^{\text{O}} \sim 50$ and $E_d^{\text{Zn}} \sim 50$ -70 eV), and UO_2 ($E_d^{\text{O}} = 20$ and $E_d^{\text{U}} \sim 40$ eV),³⁰ for non-directional measurements. Recent developments in molecular dynamics (MD) have shown that it is possible to determine an "average" value of E_d over a set of uniformly distributed directions.³¹ This method returned values for rutile (TiO_2) of $E_d^{\text{O}} = 19$ eV and $E_d^{\text{Ti}} = 69$ eV at $T = 300\ \text{K}$, similar to experimental data for UO_2 cited above. In a related paper,³² the temperature dependence of E_d for rutile was calculated from 50 to 1200 K, showing that thermal activation of Frenkel defects caused significant increases in the E_d^{O} values at high temperatures. In view of the preceding discussion, the general complications involved in determining displacement energies in solids, together with the lack of data for our samples, we believe that the results in Table 2 are justified using the "global" value of $E_d = 50$ eV. For the ABO_4 compounds used in this study, the calculated nuclear stopping power

TABLE 1 Literature data for the crystal structures,^{15–24} mean bond lengths for A-O and B-O coordination polyhedra, packing index (PI), and A-B cation ionic radius ratio (r_A/r_B), for the compounds examined in this study. Included here are our DFT results for the A-B cation anti-site defect formation energy E_{fAB} , cation charge ratio $q_{A/B}$, and oxygen charge q_O , as determined for a subset of five compounds

	YVO ₄	LaVO ₄	YNbO ₄	LaNbO ₄	CaWO ₄	SrWO ₄	BaWO ₄
Structure	Z	M	F	F	S	S	S
Space group	<i>I4₁/amd</i>	<i>P2₁/n</i>	<i>I2/a</i>	<i>I2/a</i>	<i>I4₁/a</i>	<i>I4₁/a</i>	<i>I4₁/a</i>
<i>a</i> (Å)	7.1183	7.047	5.317	5.565	5.243	5.4268	5.6065
<i>b</i> (Å)	7.1183	7.286	10.999	11.519	5.243	5.4268	5.6065
<i>c</i> (Å)	6.2893	6.725	5.090	5.202	11.376	11.9688	12.7084
β (°)	90.00	104.85	94.53	94.10	90.00	90.00	90.00
<i>V</i> (Å) ³	318.68	333.76	296.74	332.61	312.72	352.48	399.46
\langle A-O \rangle (Å)	2.3654	2.5965	2.363	2.505	2.4585	2.5405	2.724
\langle B-O \rangle (Å)	1.7088	1.7090	1.894	1.874	1.7854	1.869	1.822
ρ_{calc} (g cm ⁻³)	4.25	5.05	5.58	5.91	6.12	6.32	6.40
PI	58.70	60.33	63.41	59.11	61.84	57.69	54.52
r_A/r_B	2.870	3.268	2.123	2.417	2.667	3.000	3.714
E_{fAB} (eV)	8.25	10.58	2.48	4.04	6.58	---	---
$q_{A/B}$	1.07	1.06	0.84	0.82	0.56	---	---
q_O	-1.09	-1.07	-1.23	-1.20	-1.14	---	---

TABLE 2 Results of SRIM simulations of damage production, including the electronic (dE/dx_e) and nuclear (dE/dx_n) components of stopping power, and electronic to nuclear stopping power ratio (ENSP)

Sample	$(dE/dx)_e$ eV nm ⁻¹	$(dE/dx)_n$ eV nm ⁻¹	ENSP Ratio
YVO ₄	795	1113	0.714
LaVO ₄	872	1126	0.774
YNbO ₄	979	1342	0.730
LaNbO ₄	976	1246	0.783
CaWO ₄	801	1245	0.643
SrWO ₄	786	1201	0.654
BaWO ₄	773	1116	0.693

ranges from 1113 to 1342 eV ion⁻¹ nm⁻¹, the electronic stopping power ranges from 773 to 979 eV ion⁻¹ nm⁻¹, and the electronic-to-nuclear stopping power (ENSP) ratio ranges from 0.643 to 0.783.

3.5 | Density functional theory (DFT) simulations

Static calculations were carried out on five of the ABO₄ compounds studied here: CaWO₄ (scheelite), LaVO₄ (monazite), YVO₄ (zircon), and YNbO₄ and LaNbO₄ (fergusonite). The atomic bonding was predicted using density functional theory (DFT) within the VASP code.^{33,34} The generalized gradient approximation (GGA) with the Perdew-Burke-Ernzerhop (PBE) exchange correlation was employed together with the

projector augmented wave (PAW) pseudopotential. The DFT approach was chosen to account for the variation in bonding expected to occur as the structure and composition of the ABO₄ system is varied. An energy cutoff value of 450 eV was used together with a $2 \times 2 \times 2$ k-point grid. For each of the five compounds, representing the four different structure types noted above, the energy involved in the exchange of Ca-W, La-V, Y-V, Y-Nb, and La-Nb next-nearest-neighbor (NNN) pairs was determined. We also investigated some of the fundamentals of bonding in these compounds by calculating the A-B cation charge ratio and the effective charge on the oxygen atom. The results of these calculations are listed in Table 1.

4 | RESULTS

4.1 | Structure and composition of the ceramics

The structural details of the nominal ABO₄ compounds are shown in Table 1, based on high-quality data from the literature.^{16–24} This table also includes the A-B cation anti-site defect formation energies, E_{fAB} , calculated in this study. Figure 3 shows the XRD patterns which were in excellent agreement with the literature data. The samples were identified by laboratory XRD as essentially single-phase materials with either monoclinic or tetragonal crystal structure. Trace amounts of monoclinic ZrO₂ in the YNbO₄ sample may be indicated by very weak reflections appearing close to 28 and 31° 2 θ , probably incorporated during ball-milling. An SEM

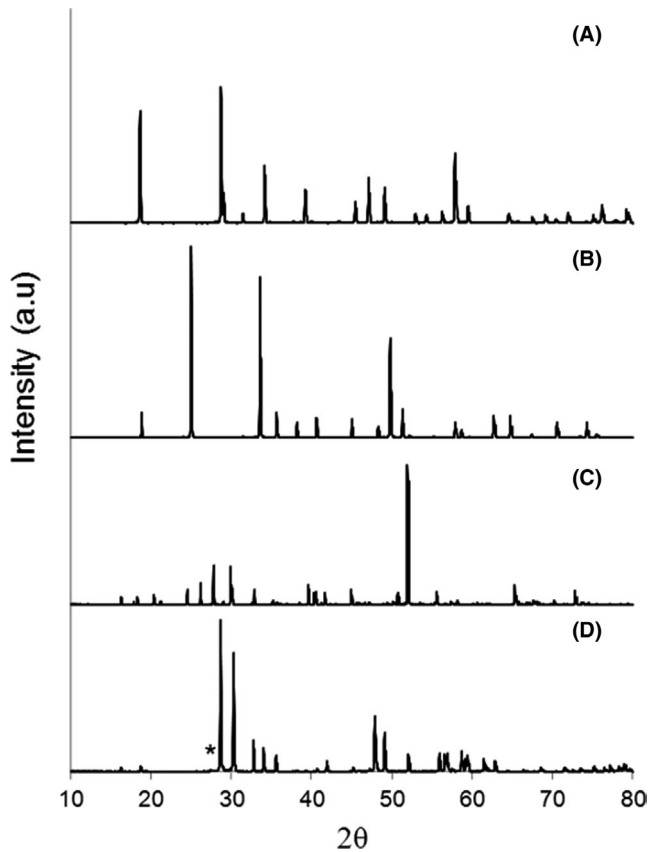


FIGURE 3 X-ray diffraction patterns of (A) CaWO_4 , (B) YVO_4 , (C) LaVO_4 , and (D) YNbO_4 . Trace monoclinic ZrO_2 is indicated by the star in (D). Otherwise, the ceramics are essentially phase pure at the level of detection typical for laboratory X-ray diffraction. The pattern shown for LaVO_4 appears to show the effects of preferred orientation in the powder sample

image collected for each sample with the backscatter detector confirmed the single-phase nature of the samples and EDS analyses verified the phase composition. There was no evidence for ZrO_2 in the SEM images collected with the backscatter detector.

4.2 | Ion irradiation

The radiation-induced crystalline-to-amorphous transition in all ABO_4 compounds was monitored through a sequence of SAED patterns, mapping the gradual decrease in Bragg intensity and complementary increase in diffuse scattering from amorphous domains under continuous irradiation, until complete amorphization was observed as diffuse halos (no Bragg beams present) above the critical amorphization fluence, F_c . This critical threshold value generally increases as a function of irradiation temperature due to the defect recombination and epitaxial recrystallization processes at elevated temperatures which suppress the amorphization process. At this point, a certain critical temperature (T_c) is reached where

the transition to complete amorphization does not occur. A plot of this relationship for the seven compounds investigated in this study can be seen in Figure 4, conferred by the expression:

In this equation, F_c is the fluence for complete amorphization at 0 K, T_c the critical temperature at which full

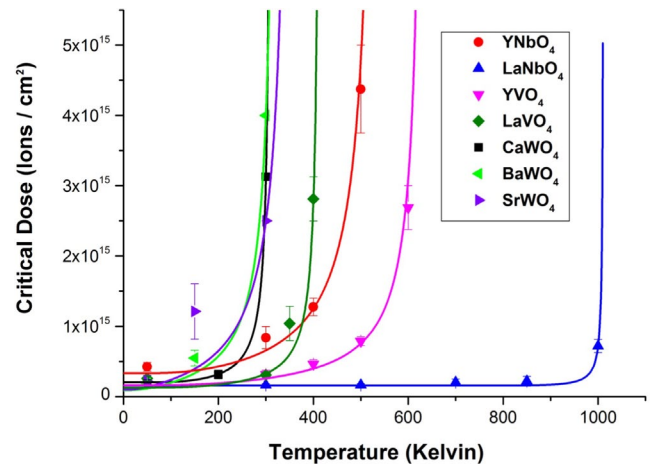


FIGURE 4 A plot of the critical dose for amorphization (D_c) as a function of temperature for the ABO_4 compounds using in situ experimental techniques and thin TEM samples. Extrapolation of the curves to infinity gives the critical temperature for amorphization. Data obtained in this study for seven vanadate, niobate, and tungstate compounds (see legend) irradiated using 1.0 MeV Kr ions. The thicknesses of the crystals are typically on the order of 60 nm (see text for further details and discussion). Results demonstrate that the critical temperatures for amorphization range from about 300 K to 1000 K overall, increasing from the three AWO_4 (scheelite) compounds to LaVO_4 (monazite) to YNbO_4 (fergusonite) to YVO_4 (zircon) to LaNbO_4 (fergusonite). The relative order of LaVO_4 is consistent with previous work on the corresponding phosphates¹² [Color figure can be viewed at wileyonlinelibrary.com]

TABLE 3 Critical amorphization fluence (F_{c0}), displacements per atom (dpa), and radiation damage cross sections (σ_a), all at zero Kelvin; together with the calculated defect annealing activation energies (E_a) and critical temperatures for amorphization (T_c) of seven ABO_4 compounds irradiated with 1.0 MeV Kr ions as a function of temperature

Sample	F_{c0} (10^{14} cm^{-2})	dpa	σ_a (10^{-14} cm^2)	E_a (eV)	T_c (K)
YVO_4	1.63	0.13	0.61	1.95	636 (26)
LaVO_4	1.30	0.22	0.77	1.26	415 (17)
YNbO_4	3.30	0.52	0.30	1.69	541 (6)
LaNbO_4	1.57	0.29	0.64	3.09	1012 (1)
CaWO_4	2.04	0.36	0.49	0.96	311 (1)
SrWO_4	1.00	0.19	1.00	1.10	358 (90)
BaWO_4	0.92	0.20	1.09	0.98	325 (19)

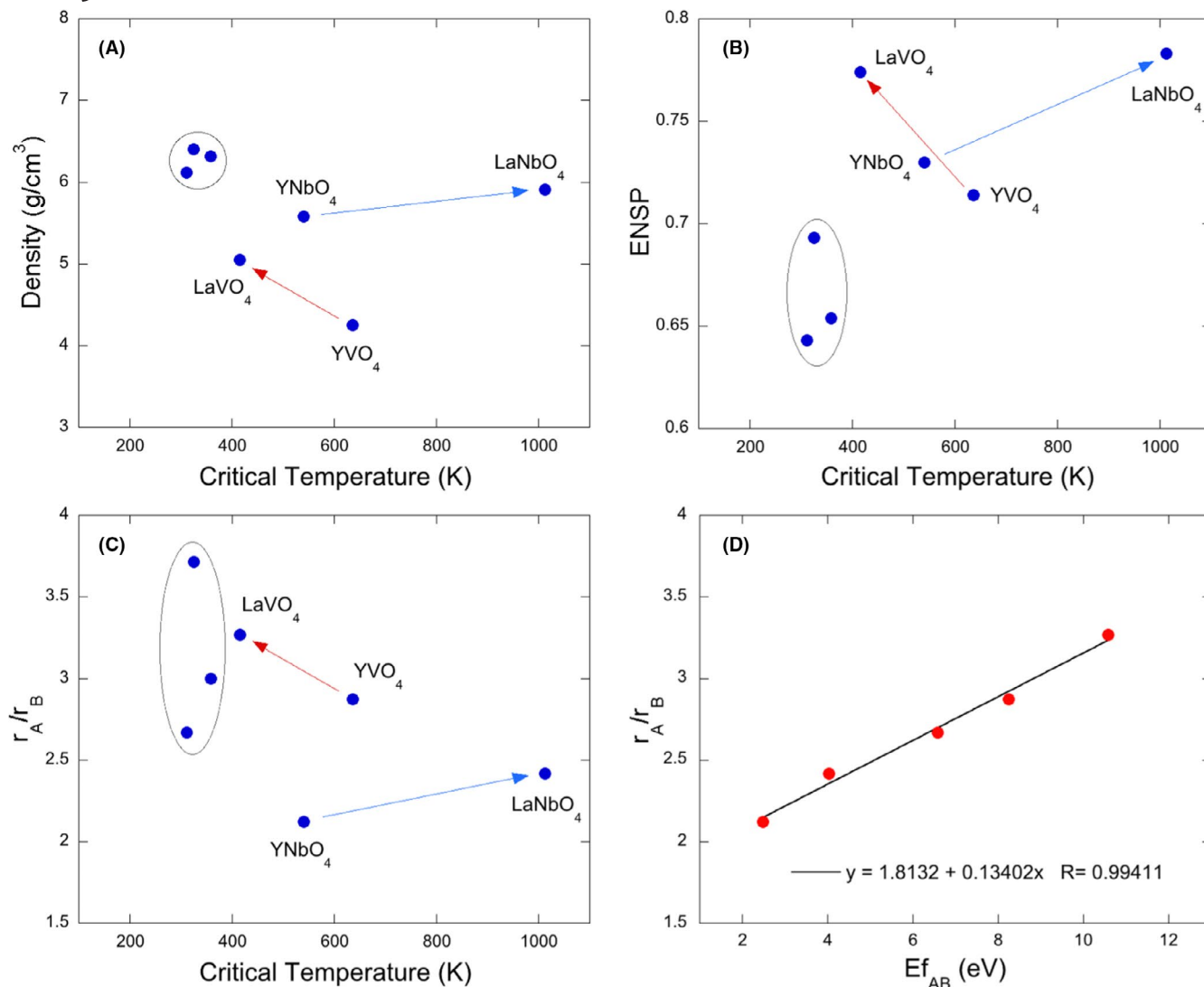


FIGURE 5 Plots of the critical temperature for amorphization (T_c) against the density in (A) and the electronic to nuclear stopping power (ENSP) in (B). The blue arrows show the possible trends of fergusonite compounds from $YNbO_4$ to $LaNbO_4$, the red arrows show the possible trends from $LaVO_4$ (monazite) to YVO_4 (zircon), and the circle and oval enclose the data for the scheelite compounds with $A = Ca, Sr, Ba$. (C) A plot of the A-B cation radius ratio (r_A/r_B) vs the critical temperature for amorphization (T_c). Arrows and oval as per figures (A) and (B) above. In (D) the relationship between the A-B cation anti-site defect formation energy ($E_{f_{AB}}$) and the A-B cation ionic radius ratio (r_A/r_B) is plotted for five of the seven compounds where we have DFT data, revealing a close relationship between these parameters [Color figure can be viewed at wileyonlinelibrary.com]

amorphization ceases, E_a the activation energy for crystalline recovery, k_b the Boltzmann constant and T the measured experimental temperature.^{35,36} Data from this refinement, including the extrapolated critical fluence at 0 K (D_{c0}), critical temperature (T_c) and defect annealing activation energy (E_a), are summarized in Table 3.

Under the stated experimental conditions, none of the compounds studied here are inherently radiation tolerant, with calculated intercept fluences of $F_{c0} = 0.9\text{--}3.3 \times 10^{14}$ ions cm^{-2} . This is equivalent to radiation damage cross-sections for amorphization $\sigma_a = 1/F_{c0} = 0.3\text{--}1.1 \times 10^{14}$ cm ion^{-1} . The low temperature behavior observed here is similar to that found for a range of complex oxides and the intercept fluences are

just below values observed for the prototypical zirconolite and titanate pyrochlore nuclear waste form compositions. Of the seven ABO_4 compounds, the three scheelite samples became amorphous below 400 K, but a systematic trend between the three compounds could not be determined due in part to the large error in the T_c determination for $SrWO_4$ (see Table 3). In contrast to this result, $LaNbO_4$ was found to be the least radiation tolerant compound with a T_c of 1012 K, followed by YVO_4 (636 K), $YNbO_4$ (541 K), and $LaVO_4$ (415 K). During ion irradiation experiments at elevated temperature, $LaNbO_4$ should go through the monoclinic-tetragonal phase transformation at ~ 763 to 798 K,³⁷ but with no apparent effect on the fluence-temperature response. Note also that we do not find

any direct evidence for complex, multi-stage recovery of damage in these materials, as was reported in a previous study.¹³

As shown in Figure 5A-C, there are broad correlations between density, the electronic to nuclear stopping power ratio (ENSP) for these irradiations, and the A-B cation ionic radius ratio (r_A/r_B). Density and r_A/r_B (Figure 5A,C) are negatively correlated with T_c for these structure types as a group, with the fergusonite data showing a general reversal in behavior from La to Y with respect to the trend shown by the two monazite (LaVO_4) and zircon (YVO_4) samples. Figure 5B, on the other hand, shows that ENSP is positively correlated with T_c from the three scheelite compounds to the group at low to medium T_c including monazite, zircon, and fergusonite (YNbO_4), and then up to fergusonite (LaNbO_4) at the highest T_c value.

4.3 | DFT calculations

The cation anti-site defect formation energies (E_{fAB}) obtained in this study are listed in Table 1 and plotted in Figure 5D and Figure 6A. In general, the energies, E_{fAB} required for an A-B cation exchange event to occur range from about 2.4 to 10.6 eV for the five ABO_4 compounds investigated here and are generally uncorrelated with T_c across the range of structure types and compositions. Interestingly, the lowest E_{fAB} values were found for the fergusonite structure type: 2.48 eV for YNbO_4 and 4.04 eV for LaNbO_4 . This range points to a possible systematic difference in cation anti-site behavior for the fergusonite structure as a function of composition. An intermediate value of $E_{fAB} = 6.58$ eV was determined for scheelite

CaWO_4 . The highest cation anti-site energies were found for the zircon and monazite structure types, YVO_4 and LaVO_4 , respectively, with $E_{fAB} = 8.25$ and 10.58 eV, respectively. Figure 5D shows that the E_{fAB} values determined for the cation anti-site energy are highly correlated with the cation radius ratio, r_A/r_B , for all samples as a group, given by the linear relationship $r_A/r_B = 0.134(E_{fAB}) + 1.8132$ with $R^2 = 0.988$.

We also calculated the A/B cation charge ratio ($q_{A/B}$) and the average charge on the oxygen atom (q_O) for each of the five different compounds (Table 1, Figure 6A,B). Overall, the A/B charge ratios determined from DFT calculations decrease systematically from the samples with B = V (zircon or monazite) to Nb (fergusonite) to W (scheelite) for which the $q_{A/B}$ values are 1.07, 1.06, 0.84, 0.82, and 0.56, respectively. The ideal ionic values of $q_{A/B}$ are 0.60 based on the formal charges, A^{3+} and B^{5+} , for the zircon, monazite, and fergusonite compounds and 0.33 based on the formal charges, A^{2+} and B^{6+} , for the scheelite compound investigated here. In terms of the corresponding value of the oxygen charge, q_O , across this series in the same order, we find that q_O decreases from -1.09 and -1.07 for the samples with B = V (zircon or monazite) to -1.23 and -1.20 for B = Nb (fergusonite) and then increases again to -1.14 for B = W (scheelite). The ideal ionic charge for O is, of course, -2.00 in these compounds.

5 | DISCUSSION

Under the conditions used for these in situ experiments all of the irradiated materials investigated in this study are

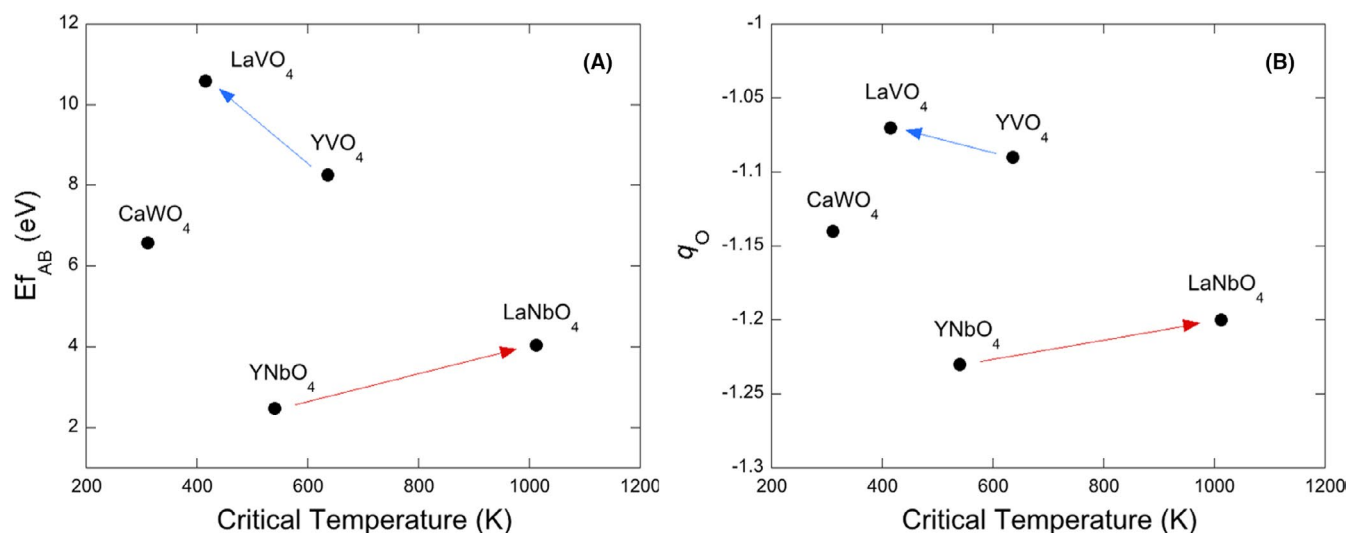


FIGURE 6 Plots obtained from experimental and DFT data showing the trends of the cation anti-site energy E_{fAB} (A) and the charge on the oxygen atoms q_O (B) for five of the compounds investigated in this study. The relationships shown here are complex due to the different structure types represented. The radiation response of CaWO_4 may be influenced by formation of O interstitials between pairs of WO_4 tetrahedra and enhanced mobility and recovery (see text). However, the results for the Y and La niobate fergusonite structures (connected by red arrows) indicate that the A-B cation anti-site energies and the more ionic character of the O atoms may play a significant role in the radiation damage recovery mechanism, similar to the related fluorite structure type [Color figure can be viewed at wileyonlinelibrary.com]

inherently susceptible to amorphization induced by the 1.0 MeV Kr ions. The intercept fluences given in Table 3, as derived from the fluence-temperature response curves, are somewhat higher than the range of $1.0\text{--}1.6 \times 10^{14}$ ions cm^{-2} reported for the monazite and xenotime (zircon) orthophosphates by Meldrum et al¹² using similar in situ irradiations but with 800 keV Kr ions. In another study using similar experimental conditions, Meldrum et al¹³ determined F_{c0} values of $1.1\text{--}1.5 \times 10^{14}$ ions cm^{-2} for the orthosilicates with the zircon (ZrSiO_4 , HfSiO_4 , ThSiO_4) and monazite ($\text{ThSiO}_4 = \text{huttonite}$) structure. Furthermore, heavy ion irradiation of ZrSiO_4 single crystals with 540 keV Pb ions at 77 K shows that complete amorphization occurs at a fluence of approximately 10^{14} ions cm^{-2} .³⁸

The factors that influence damage recovery in this complex system of structures and compositions are poorly understood; however, the temperature response based on the T_c values follows the general pattern of II-VI scheelite < III-V monazite < III-V zircon < III-V fergusonite. Furthermore, in relation to monazite and zircon, the trend in radiation response of fergusonite is reversed, ie, the compound with the largest A-site cation (La) is the least radiation tolerant. As a result of this reversal, the T_c value of YNbO_4 is significantly lower than that of YVO_4 but slightly higher than the value of 512 K reported for YPO_4 (zircon). The results of this study demonstrate that the response to external irradiation is complicated in the broader ABO_4 system. Our results demonstrate that the three scheelite samples are the most radiation tolerant compounds investigated in this study, with T_c values below that of LaPO_4 monazite.¹² The low T_c value obtained for CaWO_4 in this study is supported by the work of Mendoza et al³⁹ who conducted ion irradiations of ceramic samples of powellite (CaMoO_4 with the scheelite structure) doped with lanthanides and Na. Following ion irradiation with 8 MeV Ar ions to 1.2×10^{16} ions cm^{-2} or 108 MeV Pb ions to 10^{14} ions cm^{-2} (presumably at room temperature), the authors suggest that the crystalline structure of the powellite is retained. Based on evidence obtained from $\text{Eu}^{3+} {}^5\text{D}_0 \rightarrow {}^7\text{F}_0$ luminescence spectra, it appears that the Ar irradiations only have a minor effect on the local environment of Eu. Although the Eu local environments were randomized by the Pb irradiations, the structure of the CaMoO_4 remained crystalline.

In a study designed to simulate the effects of alpha decay damage, Picot et al⁴⁰ conducted irradiation experiments on LaPO_4 and $\text{La}_{0.73}\text{Ce}_{0.27}\text{PO}_4$ monazite ceramics using 1.7 MeV He ions to 1.2×10^{16} ions cm^{-2} and 1 MeV, 3.5 MeV, and 7 MeV Au ions to 2.3×10^{15} ions cm^{-2} . Results of the study demonstrate that $(\text{La,Ce})\text{PO}_4$ monazite can be rendered amorphous by irradiation with Au ions under these conditions and also show that it undergoes a volume expansion of ~8%. Irradiation with He ions does not generally lead to amorphization of monazite due to the small number of defects produced per ion and the associated low energy barriers

for defect recovery, but the volume does increase by ~0.8%, probably due to the accumulation of point defects in the structure. Alpha recoil nuclei from actinides and heavy ion irradiation, on the other hand, may produce damage cascades with orders of magnitude higher defect concentrations and higher energy barriers to recovery, potentially leading to amorphization over time. Natural monazites, however, are always found in the crystalline state even with high Th-U contents (over 20 wt.% in some cases) and very old geological ages. It is also known that synthetic samples doped with 8.1 wt% ²³⁸Pu remain crystalline on the time scale of the experiments (several years), showing evidence of damage accumulation and retention in the form of decreased X-ray diffraction peaks relative to the starting material (Burakov et al⁴¹). Therefore, the barriers to damage recovery are accessible and may be overcome in natural systems where monazite samples are stored for geological time periods (lower dose rate) at somewhat elevated temperatures, averaging ~100–200°C in numerous cases.^{42,43}

The recovery of damage as a function of temperature in the ABO_4 orthovanadates (A = La, Y) with the monazite and zircon structure can be compared directly with similar experiments reported previously for phosphate and silicate systems. Firstly, it is instructive to compare our results for LaVO_4 (monazite) and YVO_4 (xenotime) with the orthophosphates studied by Meldrum and coworkers.¹² Our temperature-fluence data give $T_c = 410$ K for LaVO_4 and 644 K for YVO_4 whereas Meldrum's LaPO_4 and YPO_4 samples gave $T_c = 333$ K for LaPO_4 and 512 K for YPO_4 using a slightly lower ion energy of 800 keV.¹² These results demonstrate that the vanadates studied here are probably less radiation tolerant (with respect to T_c) than the corresponding phosphates based on the critical temperature values. This is consistent with the trends observed for the thermochemistry of orthophosphate and orthovanadate compounds with the zircon and monazite structures, eg, the enthalpies of formation reported by Ushakov et al⁴⁴ and Dorogova et al⁴⁵ show that the vanadates are consistently less stable than the phosphates with respect to the oxides by ~190 kJ mol^{-1} with the light lanthanide compounds being more stable in both systems.

In the experiments conducted via in situ ion irradiation, the orthosilicates with the zircon (ZrSiO_4 , HfSiO_4 , ThSiO_4) or monazite structure type (ThSiO_4) have high T_c values on the order of 900–1200 K.¹³ This is a clear illustration of the major effect of chemistry in the IV-IV vs III-V monazite and zircon structure types. In the orthosilicates, Si probably plays a major role in the stabilization of defects via polymerization effects, forming local -Si-O-Si- units, Q^n , with $n \leq 4$. A major outcome of the polymerization of Si is local segregation of Si and A-site cations in collision cascades (eg Farnan and Salje⁴⁶). Little work has been published on radiation effects in IV-IV ABO_4 compounds with other B-site cations; however, recent results have been reported for 93 MeV Ni

irradiations conducted on ceramic samples of ThGeO_4 in both the zircon and scheelite structure types (Patel et al⁴⁷). At room temperature, these “swift heavy ion” irradiation experiments caused amorphization of the zircon and scheelite phases at fluences of 6×10^{13} and 0.75×10^{13} ions cm^{-2} , respectively. These data indicate that the radiation tolerance of the zircon structure type is greater than that of the scheelite type for the ThGeO_4 polymorphs.

Fergusonite compounds have not received much attention with regard to experimental ion irradiation damage effects, but most natural samples are found in the metamict (amorphous) state, indicating that this structure type is generally susceptible to amorphization (see Lumpkin and Geisler⁴⁸). The results of this study reveal that fergusonite is the least resistant structure type to amorphization induced by 1.0 MeV Kr ions. Furthermore, the trend in radiation tolerance with respect to A-site cation radius is reversed relative to the monazite and zircon compounds with $B = \text{P}$ and V . Based on a simple calculation using the differences in A-site cation radii and measured T_c values, we estimate that the T_c of LuNbO_4 is ~ 398 K. Thus, the range of critical temperatures for the fergusonite type niobates may span a temperature range of ~ 650 K, considerably greater than the range of ~ 250 K for the monazite and zircon orthophosphates combined.¹²

From the above discussion, the effects of 1.0 MeV Kr ion irradiation on thin crystals of the ABO_4 compounds

investigated in this study are very complicated. In spite of the complexity of the results, we observe a distinct positive correlation between ENSP and T_c for CaWO_4 , YNbO_4 , and LaNbO_4 , the three compounds with corner sharing tetrahedra. Together with the T_c values, this suggests that the electronic component of the stopping power assists in the production of defects in YNbO_4 and LaNbO_4 in particular, and that energy barriers for migration may be generally higher in the fergusonite structure type. However, embedded within the data set are the values for the monazite and zircon type orthovanadates, LaVO_4 and YVO_4 , which have calculated ENSP values of 0.77 and 0.71. Although this trend is reversed in comparison to the other three samples of this study, it is consistent with the data presented in previous work for the orthophosphates¹² wherein ENSP is negatively correlated with T_c in these compounds, an indication that electronic interactions between the Kr ions and the atoms of the crystal may assist in defect recombination during the irradiations.

Provided that we separate the data for the two fergusonite samples from the others, results of this study show that density and r_A/r_B are negatively correlated with the critical temperature for amorphization (see Figure 5). In general, these observations are consistent with previous work on the TiO_2 polymorphs, for example, where the trend in radiation tolerance is highly correlated with density, molar volume, and packing index.⁴⁹ However, the situation is much more

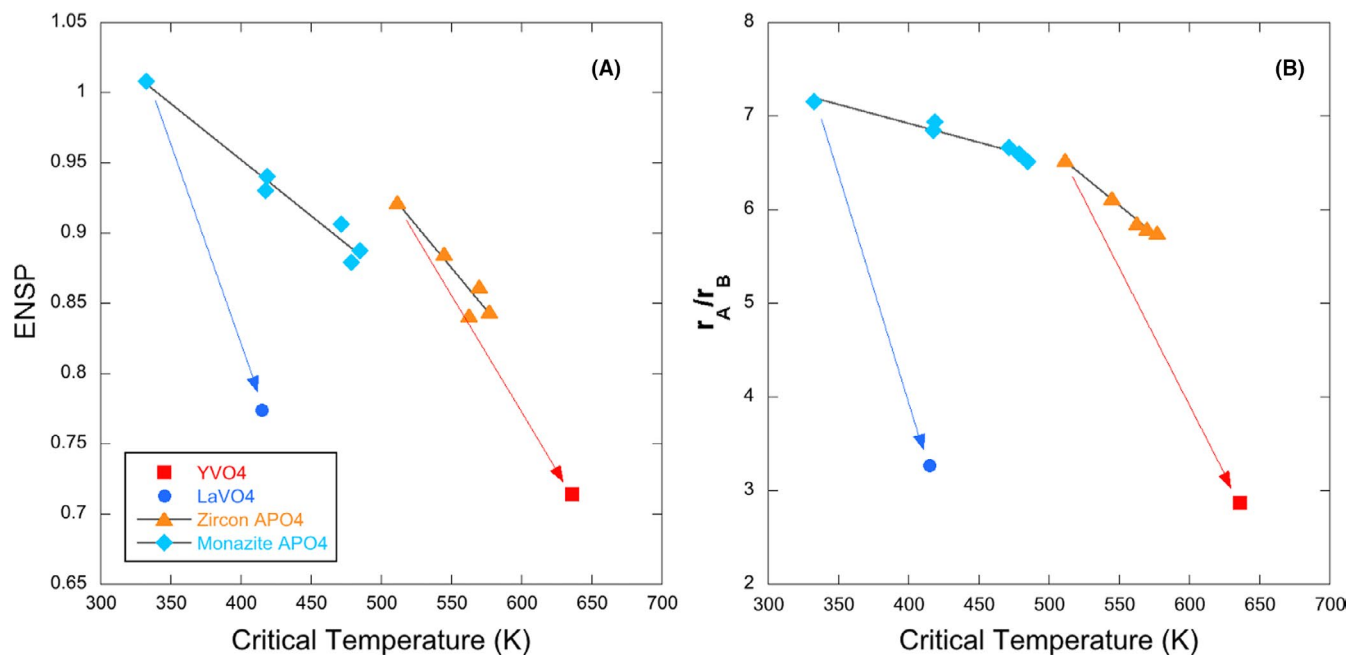


FIGURE 7 Plots of ENSP (A) and r_A/r_B (B) vs the critical temperature for amorphization (T_c) for LaVO_4 monazite (blue circle) and YVO_4 zircon (red square) compounds compared with the phosphates (monazite = blue diamonds and zircon = orange triangles) reported by Meldrum et al¹² using 0.8 MeV Kr ions using the IVEM Tandem Facility. These figures reveal the relationships between T_c and experimental and structural parameters of the phosphates in greater detail than previously reported. The monazite phosphates range from $A = \text{La}$ to Gd (highest T_c) and the zircon phosphates range from $A = \text{Y}$ to Lu (highest T_c). The blue arrow connects LaPO_4 and LaVO_4 and the red arrow connects YPO_4 and YVO_4 , providing an indication of the shifts in T_c as a function of substitution of V for P on the B-site [Color figure can be viewed at wileyonlinelibrary.com]

complex than this, eg, for the monazite and zircon type orthophosphates, ENSP is actually negatively correlated with T_c within each structure type. This is illustrated in detail in Figure 7, where we have plotted literature data for the phosphates¹² showing the variation in ENSP and r_A/r_B against T_c , clearly emphasizing the trends and, in particular, the steeper negative slopes for the zircon type orthophosphates relative to the monazites.

Finally, we have provided a view of the role of cation anti-site defect formation energies, cation charge ratio, and oxygen charge in the radiation damage of these structure types at the atomic scale using DFT calculations. Based on the values of E_{fAB} , it is unlikely that A-B cation anti-site disorder occurs to the extent that the materials transform to a disordered state, even in the case of YNbO_4 fergusonite with $E_{fAB} = 2.48$ eV. However, anti-site disorder is not the only important defect mechanism and the energetics of cation and anion Frenkel defects may play a role in radiation damage recovery. In a study of CaWO_4 , Shao et al⁵⁰ used empirical potentials to determine Frenkel defect energies of 1.23 eV for O and 4.04 eV for Ca. The Frenkel pair defect energy for a W vacancy and interstitial were not reported; however, data were presented suggesting that O atoms and vacancies have low migration energies of ~ 0.2 eV along 4 of the six WO_4 tetrahedral edges in the structure. This is generally consistent with experimental data and other atomistic studies of scheelite and related structure types^{51,52} and may play a role in determining the radiation damage recovery as a function of temperature. Another potential mechanism for oxygen migration in scheelite structures was identified by Wang et al⁵³ who used molecular dynamics to study interstitial oxide ion migration in $\text{Pb}_{1-x}\text{La}_x\text{WO}_{4+x/2}$ compounds. In these materials, which contain extra oxygen with La doping, it was found that the lowest energy interstitial site for oxygen is on coordinates (0.5, 0.5, 0.5) of the unit cell between two WO_4 tetrahedra. The simulations also indicate that O atoms may migrate between the different tetrahedral units of the structure. This mechanism could also be operative in stoichiometric scheelites under irradiation, initiated by O displacements. In comparison with the above results, Yi et al⁵⁴ used DFT methods to calculate Frenkel defect formation energies of 12.4 eV and 11.0 eV for Ce and O, respectively, in CePO_4 with the monazite structure. These results indicate that there are significant differences in the energetics of defect formation and potential migration mechanisms between the scheelite and monazite structure types relevant to recovery processes during irradiation. Additionally, it was recently⁵⁵ demonstrated that the threshold displacement energy of O in LaPO_4 monazite is only 8 eV, much lower than the values obtained for La (56 eV) and P (75 eV). This raises interesting questions about the behavior of the cation and anion sublattices across the different ABO_4 structure types

during irradiation and requires further experimental and detailed atomistic simulation work.

6 | IMPLICATIONS

None of the ABO_4 compounds studied here are inherently radiation tolerant with respect to in situ 1 MeV Kr irradiation, returning damage cross-sections for amorphization given as $\sigma_a = 1/F_{c0} = 0.3\text{--}1.1 \times 14 \text{ cm}^2 \text{ ion}^{-1}$ on extrapolation to zero Kelvin. However, there are significant differences in the temperature response of the compounds, following the order II-VI scheelite < III-V monazite < III-V zircon < III-V fergusonite based on the critical temperature for amorphization (T_c). Previous work on the zircon structure silicates (ZrSiO_4 , ThSiO_4 , and USiO_4), all with T_c values near 1000 K under similar irradiation conditions, demonstrates that radiation damage recovery and post-recovery processes, eg, due to annealing and/or long-term storage, are strongly influenced by Si-Si polymerization due to the strong sp^3 orbitals. This is not an important factor in this study, with more ionic B-site cations such as V, Nb, and W.

The A-B cation anti-site energies, E_{fAB} , determined by DFT range from 2.48 to 10.58 eV and are positively correlated with the A-B cation ionic radius ratio, r_A/r_B , but are not correlated with T_c across the different structure types, consistent with the observation that none of the materials disorder during irradiation; nor do they have stable disordered structures as a function of temperature, pressure, and composition within the range of experimental conditions used here. These observations suggest that Frenkel defects play a more important role in damage recovery in these compounds, consistent with a limited set of published data. In particular, previously identified O migration behavior of scheelite with low energy jumps between sites associated with WO_4 tetrahedra, combined with the intermediate ionic character found here may play a major role in damage recovery. In contrast, the lowest E_{fAB} and q_0 values are found for the fergusonite structure and have a positive correlation with T_c over a range of 471 K, in which case a significant role in damage recovery is likely and may be a reflection of the structural similarity to fluorite.

ORCID

Robert D. Aughterson  <https://orcid.org/0000-0002-1704-024X>

Daniel J. Gregg  <https://orcid.org/0000-0003-4703-7217>

Gregory R. Lumpkin  <https://orcid.org/0000-0002-9266-0457>

REFERENCES

1. Murty KL, Charit I. Structural materials for Gen-IV nuclear reactors: challenges and opportunities. *J Nucl Mater.* 2008;383(1–2):189–95.

2. Zinkle SJ. Advanced materials for fusion technology. *Fusion Eng Des.* 2005;74(1-4):31-40.
3. Allen TR, Gan J, Cole JJ, Miller MK, Busby JT, Shutthanandan S, et al. Radiation response of a 9 chromium oxide dispersion strengthened steel to heavy ion irradiation. *J Nucl Mater.* 2008;375(1):26-37.
4. Lumpkin GR. Ceramic waste forms for actinides. *Elements.* 2006;2:365-72.
5. Stefanovsky SV, Yudinsev SV, Gieré R, Lumpkin GR. Nuclear waste forms. In: Gieré R, Stille P, editors. *Energy, waste, and the environment.* London: The Geological Society. Special. Publication 236, 2004; p. 37-64.
6. Ewing RC. Ceramic matrices for plutonium disposition. *Prog Nucl Energy.* 2007;49:635-43.
7. Lumpkin GR, Ewing RC. Geochemical alteration of pyrochlore group minerals: pyrochlore subgroup. *Am Mineral.* 1995;80:732-43.
8. Sickafus K, Minervini EL, Grimes RW, Valdez JA, Ishimaru M, Li F, et al. Radiation tolerance of complex oxides. *Science.* 2000;289:748-51.
9. Wang LM, Wang SX, Gong WL, Ewing RC, Weber WJ. Amorphization of ceramic materials by ion beam irradiation. *Mater Sci Eng.* 1998;253:106-13.
10. Finch RJ, Hanchar JM. Structure and chemistry of zircon and zircon group minerals. In: Hanchar JM, Hoskin PWO, editors. *Reviews in Mineralogy and Geochemistry, Volume 53,* 2003; p. 1-25.
11. Krumpel AH, Boutinaud P, van der Kolk E, Dorenbos P. Charge transfer transitions in the transition metal oxides $ABO_4 \cdot Ln^{3+}$ and $APO_4 \cdot Ln^{3+}$ ($A = La, Gd, Y, Lu, Sc$; $B = V, Nb, Ta$; $Ln =$ lanthanide). *J Lumin.* 2010;130(8):1357-65.
12. Meldrum A, Boatner LA, Ewing RC. Displacive radiation effects in the monazite- and zircon-structure orthophosphates. *Phys Rev B.* 1997;56:13805.
13. Meldrum A, Zinkle SJ, Boatner LA, Ewing RC. A transient liquid like phase in the displacement cascades of zircon, hafnon and thorite. *Nature.* 1998;395:56-8.
14. Meldrum A, Boatner LA, Zinkle SJ, Wang SX, Wang LM, Ewing RC. Effects of dose rate and temperature on the crystalline-to-metamict transformation in the ABO_4 orthosilicates. *Can Mineral.* 1999;37:207-21.
15. Chakoumakos BC, Abraham MM, Boatner LA. Crystal structure refinements of zircon-type MVO_4 ($M = Sc, Y, Ce, Pr, Nd, Tb, Ho, Er, Tm, Yb, Lu$). *J Sol State Chem.* 1994;109:197-202.
16. Dacheux N, Clavier N, Podor R. Versatile Monazite: Resolving geological records and solving challenges in materials science: Monazite as a promising long-term radioactive waste matrix: Benefits of high-structural flexibility and chemical durability. *Am Mineral.* 2013;98:833-47.
17. Gurmen E, Daniels E, King JS. Crystal structure refinement of $SrMoO_4$, $SrWO_4$, $CaMoO_4$, and $BaWO_4$ by neutron diffraction. *J Chem Phys.* 1971;55:1093-7.
18. Rice CE, Robinson WR. Lanthanum orthovanadate. *Acta Cryst B.* 1976;32:2232-3.
19. Weitzel H, Schröcke H. Kristallstrukturverfeinerungen von euxenite, $Y(Nb_{0.5}Ti_{0.5})_2O_6$, und M-fergusonit, $YNbO_4$. *Z Krist.* 1980;152:69-82.
20. Tsunekawa S, Kamiyama T, Sasaki K, Asano H, Fukuda T. Precise structure analysis by neutron diffraction for $RNbO_4$ and distortion of NbO_4 tetrahedra. *Acta Cryst A.* 1993;49:595-600.
21. Kay MI, Frazer BC, Almodovar I. Neutron diffraction refinement of $CaWO_4$. *J Chem Phys.* 1964;40(2):504-6.
22. Culver SP, Greaney MJ, Tinoco A, Brutchey RL. Low-temperature synthesis of homogeneous solid solutions of scheelite-structured $Ca_{1-x}Sr_xWO_4$ and $Sr_{1-x}Ba_xWO_4$ nanocrystals. *Dalton Trans.* 2015;44:15042-8.
23. Sarin P, Hughes RW, Lowry DR, Apostolov ZD, Kriven WM. High-temperature properties and ferroelastic phase transitions in rare-earth niobates ($LnNbO_4$). *J Am Ceram Soc.* 2014;97:3307-19.
24. Mariathasan JWE, Finger LW, Hazen RM. High-pressure behavior of $LaNbO_4$. *Acta Cryst B.* 1985;41:179-84.
25. Li M, Kirk MA, Baldo PM, Ryan EA. TEM with in situ ion-irradiation of nuclear materials: the IVEM-Tandem User Facility. *Microsc Microanal.* 2015;21(S3):437-.
26. Smith KL, Zaluzec NJ, Lumpkin GR. In situ studies of ion irradiated zirconolite, pyrochlore and perovskite. *J Nucl Mater.* 1997;250:36-52.
27. Lumpkin GR, Whittle KR, Rios S, Smith KL, Zaluzec NJ. Temperature dependence of ion irradiation damage in the pyrochlores $La_2Zr_2O_7$ and $La_2Hf_2O_7$. *J Phys Condens Matter.* 2004;16:8557-70.
28. Ziegler JF, Ziegler MD, Biersack JP. SRIM - The stopping and range of ions in matter. *Nucl Instr Meth Phys Res B.* 2010;268:1818-23.
29. Ziegler JF, Biersack JP, Littmark U. The stopping and range of ions in matter. New York, NY: Pergamon Press; 1985.
30. Zinkle SJ, Kinoshita C. Defect production in ceramics. *J Nucl Mater.* 1997;251(1-2):200-17.
31. Robinson M, Marks NA, Whittle KR, Lumpkin GR. Systematic calculation of threshold displacement energies: case study in rutile. *Phys Rev B.* 2012;85:104105.
32. Robinson M, Marks NA, Lumpkin GR. Sensitivity of the threshold displacement energy to temperature and time. *Phys Rev B.* 2012;86:134105.
33. Kresse G, Furthmüller J. Efficient iterative schemes for ab initio total-energy calculations using a plane-wave basis set. *Phys Rev B.* 1996;54:11169-86.
34. Kuo EY, Qin MJ, Thorogood GJ, Huai P, Ren CL, Lumpkin GR, et al. Transmutation of ABO_4 compounds incorporating technetium-99 and caesium-137. *Modelling Simul Mater Sci Eng.* 2017;25:025011.
35. Weber WJ. Models and mechanisms of irradiation-induced amorphization in ceramics. *Nucl Instr Meth Phys Res.* 2000;166-167:98-106.
36. Wang SX, Wang LM, Ewing RC. Nano-scale glass formation in pyrochlore by heavy ion irradiation. *J Non-Cryst Sol.* 2000;274:238-43.
37. Jian L, Wayman CM. Monoclinic-to-tetragonal phase transformation in a ceramic rare-earth orthoniobate, $LaNbO_4$. *J Am Ceram Soc.* 1997;80(3):803-6.
38. Oliver C, McCallum JC, Chakoumakos BC, Boatner LA. Hardness and elastic modulus of zircon as a function of heavy-particle irradiation dose: II. Pb-ion implantation damage. *Rad Eff Def Sol.* 1994;132:131-41.
39. Mendoza C, de Ligny D, Panczer G, Peugeot S, Bardez Giboire I, Schuller S. Behaviour of the $Eu^{3+} {}^5D_0 \rightarrow {}^7F_0$ transition in $CaMoO_4$ powellite type ceramics under Ar and Pb ions implantation. *Opt Mater.* 2011;34:386-90.
40. Picot V, Deschanel X, Peugeot S, Glorieux B, Seydoux-Guillaume AM, Wirth R. Ion beam radiation effects in monazite. *J Nucl Mater.* 2008;381:290-6.

41. Burakov BE, Yagovkina MA, Pankov AS. Behavior of zircon based ceramic doped with ^{238}Pu under self-irradiation. Conference Transactions, Plutonium Futures – The Science. 2003;274–5.
42. Lumpkin GR, Smith KL, Blackford MG, Gieré R, Williams CT. The crystalline-amorphous transformation in natural zirconolite: evidence for long-term annealing. In: McKinley G, McCombie C, editors. Scientific Basis for Nuclear Waste Management XXI, Warrendale, PA: Materials Research Society Proceedings; 1998, Vol. 506, 215–22.
43. Lumpkin GR, Day RA, McGlenn PJ, Payne TE, Gieré R, Williams CT. Investigation of the long-term performance of betafite and zirconolite in hydrothermal veins from Adamello, Italy. In: Wronkiewicz DJ, Lee JH, editors. Scientific Basis for Nuclear Waste Management XXII, Warrendale, PA: Materials Research Society Proceedings; 1999, Vol. 556, 793–800.
44. Ushakov SV, Helean KB, Navrotsky A, Boatner LA. Thermochemistry of rare earth orthophosphates. *J Mater Res.* 2001;16:2623–33.
45. Dorogova M, Navrotsky A, Boatner LA. Enthalpies of formation of rare earth orthovanadates, REVO_4 . *J Sol State Chem.* 2007;180:847–51.
46. Farnan I, Salje EKH. The degree and nature of radiation damage in zircon observed by ^{29}Si nuclear magnetic resonance. *J Appl Phys.* 2001;89:2084–90.
47. Patel MK, Avasthi DK, Kulriya PK, Kailas S, Pivin JC, Tyagi AK, et al. Swift heavy ion induced structural modifications in zircon and scheelite phases of ThGeO_4 . *Nucl Instr Meth Phys Res B.* 2010;268:42–8.
48. Lumpkin GR, Geisler-Wierwille T. Minerals and natural analogues. In: Konings RJM, editor. Comprehensive Nuclear Materials. Amsterdam: Elsevier; 2012, Vol. 5, p. 563–600.
49. Lumpkin GR, Smith KL, Blackford MG, Thomas BS, Whittle KR. Experimental and atomistic modelling study of ion irradiation damage in thin crystals of the TiO_2 polymorphs. *Phys Rev B.* 2008;77:214201.
50. Shao Z, Zhang Q, Liu T, Chen J. Computer study of intrinsic defects in CaWO_4 . *Nucl Instr Meth Phys Res B.* 2008;266:797–801.
51. Yang X, Fernández-Carrión AJ, Wang J, Porcher F, Fayon F, Allix M, et al. Cooperative mechanisms of oxygen vacancy stabilization and migration in the isolated tetrahedral anion scheelite structure. *Nature Comm.* 2018;9:4484.
52. Li C, Bayliss RD, Skinner SJ. Crystal structure and potential interstitial oxide conductivity of LnNbO_4 and $\text{LnNb}_{0.92}\text{W}_{0.08}\text{O}_{4.04}$ ($\text{Ln} = \text{La, Pr, Nd}$). *Sol State Ionics.* 2014;262:530–35.
53. Wang J, Zhou L, Wang Y, Xu J, Yang X, Kuang X. Molecular dynamic simulation of interstitial oxide ion migration in $\text{Pb}_{1-x}\text{La}_x\text{WO}_4+x/2$ scheelite. *J Sol State Chem.* 2018;268:16–21.
54. Yi Y, Zhao X, Teng Y, Bi B, Wang L, Wu L, et al. First-principles study of point defects in CePO_4 monazite. *J Nucl Mater.* 2016;482:170–4.
55. Ji Y, Kowalski PM, Neumeier S, Deissmann G, Kulriya PK, Gale JD. Atomistic modeling and experimental studies of radiation damage in monazite-type LaPO_4 ceramics. *Nucl Instr Meth Phys Res B.* 2017;393:54–8.
56. Aldred AT. Crystal chemistry of ABO_4 compounds. In: Barney GS, Navratil JD, Schultz WW, editors. Geochemical behavior of disposed radioactive waste. Seattle, Washington: American Chemical Society, 1984, p. 305–14.

How to cite this article: de los Reyes M, Aughterson RD, Gregg DJ, et al. Ion beam irradiation of ABO_4 compounds with the fergusonite, monazite, scheelite, and zircon structures. *J Am Ceram Soc.* 2020;103:5502–5514. <https://doi.org/10.1111/jace.17288>